10-2016

Sn Vacancies in Photorefractive Sn₂P₂S₆ Crystals: An Electron Paramagnetic Resonance Study of an Optically Active Hole Trap

Eric M. Golden

Sergey A. Basun

D. R. Evans

A. A. Grabar

I. M. Stoika

See next page for additional authors

Authors

Eric M. Golden, Sergey A. Basun, D. R. Evans, A. A. Grabar, I. M. Stoika, Nancy C. Giles, and Larry E. Halliburton

E. M. Golden, S. A. Basun, D. R. Evans, A. A. Grabar (iD), I. M. Stoika, N. C. Giles, and L. E. Halliburton

View Online   Export Citation   CrossMark

Sn vacancies in photorefractive $Sn_2P_2S_6$ crystals: An electron paramagnetic resonance study of an optically active hole trap

E. M. Golden,[1] S. A. Basun,[2,3] D. R. Evans,[3] A. A. Grabar,[4] I. M. Stoika,[4] N. C. Giles,[1] and L. E. Halliburton[2,5,a)]

[1]*Department of Engineering Physics, Air Force Institute of Technology, Wright-Patterson Air Force Base, Ohio 45433, USA*
[2]*Azimuth Corporation, 4027 Colonel Glenn Highway, Suite 230, Beavercreek, Ohio 45431, USA*
[3]*Air Force Research Laboratory, Materials and Manufacturing Directorate, Wright-Patterson Air Force Base, Ohio 45433, USA*
[4]*Institute of Solid State Physics and Chemistry, Uzhgorod National University, 88 000 Uzhgorod, Ukraine*
[5]*Department of Physics and Astronomy, West Virginia University, Morgantown, West Virginia 26506, USA*

Electron paramagnetic resonance (EPR) is used to identify the singly ionized charge state of the Sn vacancy (V_{Sn}^-) in single crystals of $Sn_2P_2S_6$ (often referred to as SPS). These vacancies, acting as a hole trap, are expected to be important participants in the photorefractive effect observed in undoped SPS crystals. In as-grown crystals, the Sn vacancies are doubly ionized (V_{Sn}^{2-}) with no unpaired spins. They are then converted to a stable EPR-active state when an electron is removed (i.e., a hole is trapped) during an illumination below 100 K with 633 nm laser light. The resulting EPR spectrum has g-matrix principal values of 2.0079, 2.0231, and 1.9717. There are resolved hyperfine interactions with two P neighbors and one Sn neighbor. The isotropic portions of these hyperfine matrices are 167 and 79 MHz for the two ^{31}P neighbors and 8504 MHz for the one Sn neighbor (this latter value is the average for ^{117}Sn and ^{119}Sn). These V_{Sn}^- vacancies are shallow acceptors with the hole occupying a diffuse wave function that overlaps the neighboring Sn^{2+} ion and $(P_2S_6)^{4-}$ anionic unit. Using a general-order kinetics approach, an analysis of isothermal decay curves of the V_{Sn}^- EPR spectrum in the 107–115 K region gives an activation energy of 283 meV. *Published by AIP Publishing.* [http://dx.doi.org/10.1063/1.4963825]

I. INTRODUCTION

Single crystals of $Sn_2P_2S_6$ (denoted herein simply as SPS) are semiconductors with a room-temperature optical absorption edge near 530 nm. Although basic studies of the lattice dynamics associated with the paraelectric-to-ferro-electric phase transition near 64 °C are continuing,[1–5] much of the recent interest in this material has been focused on its photorefractive applications in the red and near-infrared spectral regions.[6–23] Fast response times and high gain factors make SPS a potentially attractive photorefractive material, but little detailed information is presently available about the optically active point defects in these crystals. With the goal of optimizing the photorefractive response of the SPS crystals, we have initiated an experimental electron paramagnetic resonance (EPR) research program to identify and characterize all of the relevant electron and hole traps (i.e., shallow donors and acceptors). These efforts complement on-going computational studies of the electronic structure of intrinsic vacancies and polarons.[24–27]

The EPR technique, with its high resolution and high sensitivity, is well suited to investigate photoinduced defects in SPS crystals that have an unpaired spin.[28,29] Often, donors and acceptors in as-grown semiconducting crystals do not initially have unpaired spins (because of compensation)

and are not detected in EPR experiments. These materials, such as SPS, must be illuminated with near-band-edge light to generate "free" electrons and holes that can then be stably trapped at the pre-existing defects when the temperature is sufficiently low. This experimental approach results in observable paramagnetic charge states of acceptors and donors in SPS crystals. Thus far, two photoinduced centers representing trapped electrons and one photoinduced center representing a trapped hole have been reported. The two trapped-electron centers are singly ionized sulfur vacancies (V_S^+) and Sb^{2+} impurities substituting for Sn^{2+} ions.[30,31] The trapped-hole center is the intrinsic small polaron (Sn^{3+} ions) at Sn^{2+} sites.[32]

In this paper, we focus on native defects in nominally undoped SPS crystals, and in particular, on Sn vacancies. The Sn vacancies are a shallow acceptor in SPS and thus provide an important trap for holes when gratings are written in photorefractive experiments. Crystals were deliberately grown Sn deficient to enhance the concentration of isolated Sn vacancies. Exposing these crystals to 633 nm laser light while they are held at a temperature below 100 K converts doubly ionized Sn vacancies (V_{Sn}^{2-}) to paramagnetic singly ionized vacancies (V_{Sn}^-). The EPR spectra from these "trapped-hole centers" show well-resolved hyperfine interactions with ^{31}P nuclei at two P sites and ^{117}Sn and ^{119}Sn nuclei at one Sn site, thus indicating that the wave function of the unpaired spin is relatively diffuse. A g matrix and sets of hyperfine parameters for the ^{31}P, ^{117}Sn, and ^{119}Sn nuclei

a)Author to whom correspondence should be addressed. Electronic mail: Larry.Halliburton@ mail.wvu.edu

are obtained from the angular dependence of the EPR spectra. The thermal stability of the singly ionized charge state of the Sn vacancy is also investigated. Information about the decay kinetics and thermal activation energy of the V_{Sn}^- center is acquired from a set of isothermal decay curves taken at different temperatures in the 107–115 K region (they represent the decreasing intensity of the EPR signal when the laser light is removed).

II. EXPERIMENTAL DETAILS

Large single-crystal boules of SPS for use in the present investigation were grown by the vertical Bridgman method at Uzhgorod National University (Ukraine). Previously sintered polycrystalline starting material and a small oriented seed crystal were sealed in a quartz ampoule 7–8 cm long. The relative amounts of Sn, P, and S in the starting material were adjusted to produce SPS crystals deficient in Sn. Many of the results in this paper were obtained from a $Sn_{1.93}P_{2.03}S_{6.04}$ starting mixture (the final amounts of Sn, P, and S in this as-grown crystal are not expected to be in these same proportions). Hot and cold zones were 1120 and 870 K, respectively, and the ampoule moved at a rate of 1.5 mm/day. The boules were slowly cooled after crystallization, with a pause of several days in the 500–600 K region. This method produces single crystals with lengths of 2–3 cm and diameters of 1.2–1.5 cm. To the eye, the as-grown crystals appear slightly orange. In addition to the Sn vacancies, significant concentrations of sulfur vacancies were present in all of the Sn-deficient crystals. Also, Sb impurities (unintentionally present) were found in several of the crystals.[31] It is noteworthy that we observe the EPR signals from Sn vacancies in a variety of SPS crystals, including stoichiometric Bridgman-grown crystals and vapor-transport-grown crystals (i.e., not just Sn-deficient Bridgman crystals), thus giving our study a broader impact.

Samples for the EPR experiments were cut from the larger boules. Typical dimensions for these samples were $2.0 \times 2.5 \times 2.5$ mm^3. A Bruker EMX spectrometer operating at X band (near 9.5 GHz) was used to obtain the EPR spectra while an Oxford helium-gas flow system controlled the sample temperature. The nonparamagnetic point defects initially present in the crystals were converted to a paramagnetic charge state during an exposure at low temperature to 633 nm light from a He-Ne laser (these illuminations occurred with the sample in the microwave cavity).

Below the paraelectric-ferroelectric phase change at 64 °C, $Sn_2P_2S_6$ crystals are monoclinic (with space group Pn and point group m). Lattice constants at room temperature are $a = 9.378$ Å, $b = 7.488$ Å, $c = 6.513$ Å, and $\beta = 91.15°$, with the b axis perpendicular to the mirror plane of the crystal.[33,34] We disregard the slight deviation from 90° between the a and c axes in our analysis of the angular dependence of the EPR spectra. The $(P_2S_6)^{4-}$ anionic groups exhibit strong covalent behavior and are separated by the more ionic Sn^{2+} ions.[35] There are two slightly inequivalent tin sites, two slightly inequivalent phosphorus sites, and six inequivalent sulfur sites in the low-temperature phase of this material. In the high temperature phase (above 64 °C), the two tin sites are equivalent and the two phosphorus sites are equivalent.

III. RESULTS

A. EPR spectra

Photoinduced EPR spectra of native defects in SPS crystals often have characteristic hyperfine patterns resulting from the interactions of the unpaired electron with the nearby nuclei that have a magnetic moment (i.e., those with I > 0). These hyperfine interactions, when resolved in the EPR spectra, allow detailed models of the responsible defects to be established. Phosphorus has one isotope with a magnetic nucleus (^{31}P is 100% abundant) and tin has two isotopes with magnetic nuclei (^{117}Sn is 7.68% abundant and ^{119}Sn is 8.59% abundant). These three nuclei each have an I = 1/2 nuclear spin, and thus there are no nuclear electric quadrupole effects in the EPR spectra. The ^{115}Sn and ^{33}S nuclei also have nonzero magnetic moments, but they are neglected in the present study because of their low natural abundances (0.34% and 0.75%, respectively).

Figure 1 shows photoinduced EPR spectra from the S = 1/2 singly ionized Sn vacancy (V_{Sn}^-) in a Sn-deficient $Sn_2P_2S_6$ crystal. These data were taken at 90 K with the magnetic field aligned in succession along the a, b, and c directions in the crystal. The crystal was exposed to 633 nm laser light while each spectrum was recorded. As indicated by the stick diagram above each spectrum in Fig. 1, the Sn vacancy has a well-resolved anisotropic four-line pattern due to hyperfine interactions with two ^{31}P nuclei. Because these hyperfine interactions with the two ^{31}P nuclei are inequivalent, the EPR spectrum consists of four equally intense lines (instead of the common three-line pattern with 1:2:1 intensities normally produced by equal interactions with two I = 1/2 nuclei). Singly ionized sulfur vacancies (V_S^+) are also present in each EPR spectrum in Fig. 1. From an earlier investigation by Golden *et al.*,[30] all of the principal g values of the sulfur-vacancy EPR spectrum are known to be less than 2.0023 (i.e., they have negative g shifts relative to the free spin value), which places these sulfur-vacancy lines on the high-field side of the Sn vacancy signals. Although not shown, the sets of less-intense lines representing the hyperfine interactions of the sulfur vacancies with ^{117}Sn and ^{119}Sn nuclei at two neighboring Sn sites[30] are present approximately 19.5 mT above the primary V_S^+ line in each spectrum in Fig. 1. Defects responsible for the remaining additional weak EPR lines in Fig. 1 have not been identified.

In addition to the groups of EPR lines near g ≈ 2.0 that are shown in Fig. 1, the V_{Sn}^- defect in SPS has related but less intense EPR lines at higher magnetic field in the 435 to 460 mT region. These high-field lines are shown in Fig. 2 for each of the three crystal directions a, b, and c. They are assigned to hyperfine interactions of the V_{Sn}^- center with ^{117}Sn and ^{119}Sn nuclei at one neighboring Sn site (both of these Sn isotopes have I = 1/2). Because the sum of the natural abundances of the ^{117}Sn and ^{119}Sn nuclei is much less than 100%, the more intense lines in Fig. 1 (near g ≈ 2.0) are due to Sn vacancies that have a Sn ion with an I = 0 nucleus (either ^{116}Sn, ^{118}Sn, or ^{120}Sn) at this one participating neighboring Sn
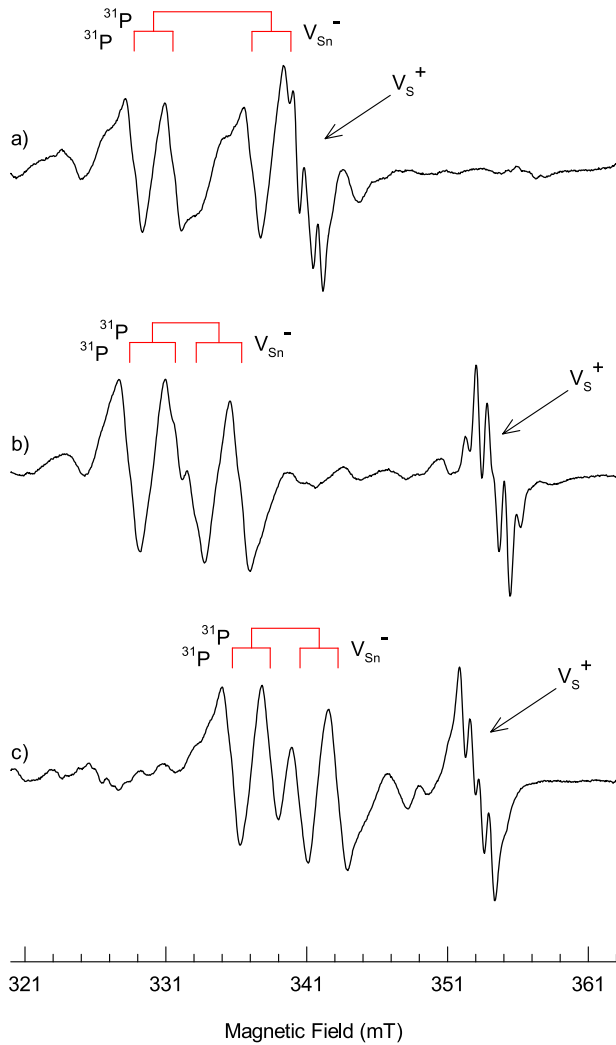
FIG. 1. EPR spectra from singly ionized Sn vacancies in a Sn-deficient $Sn_2P_2S_6$ crystal. Stick diagrams above the spectra indicate the ^{31}P hyperfine lines from the two inequivalent phosphorus neighbors. These data were taken at 90 K with a microwave frequency of 9.393 GHz. The sample was exposed to 633 nm laser light while acquiring the spectra. (a) Magnetic field along the *a* direction. (b) Magnetic field along the *b* direction. (c) Magnetic field along the *c* direction.

site. Each spectrum in Fig. 2 exhibits a hyperfine pattern from two ^{31}P interactions that is identical to the four-line pattern found in the center group in Fig. 1, as well as hyperfine split-tings due to the [117]Sn and [119]Sn interactions. Because these [117]Sn and [119]Sn interactions are resolved, there are two sets of four hyperfine lines, instead of one set of four lines, in each high-field spectrum in Fig. 2 (the [119]Sn nuclei have a slightly larger magnetic moment than the [117]Sn nuclei, thus the sets of [119]Sn hyperfine lines are seen at higher magnetic field).

Lower-field sets of [117,119]Sn hyperfine lines, counter-parts to the higher-field sets in Fig. 2, are located at magnetic fields between 35 and 80 mT. Figure 3 shows these low-field lines when the magnetic field is aligned along the *a* direction. Unlike the higher-field lines in Fig. 2, the lines in Fig. 3 are well separated into two sets of four lines, one set for the [117]Sn nuclei and one set for the [119]Sn nuclei. Each set shows the identical four-line hyperfine pattern from the two ^{31}P interactions that is seen in Fig. 1(a). We are able to observe these low-field lines for all directions of magnetic field
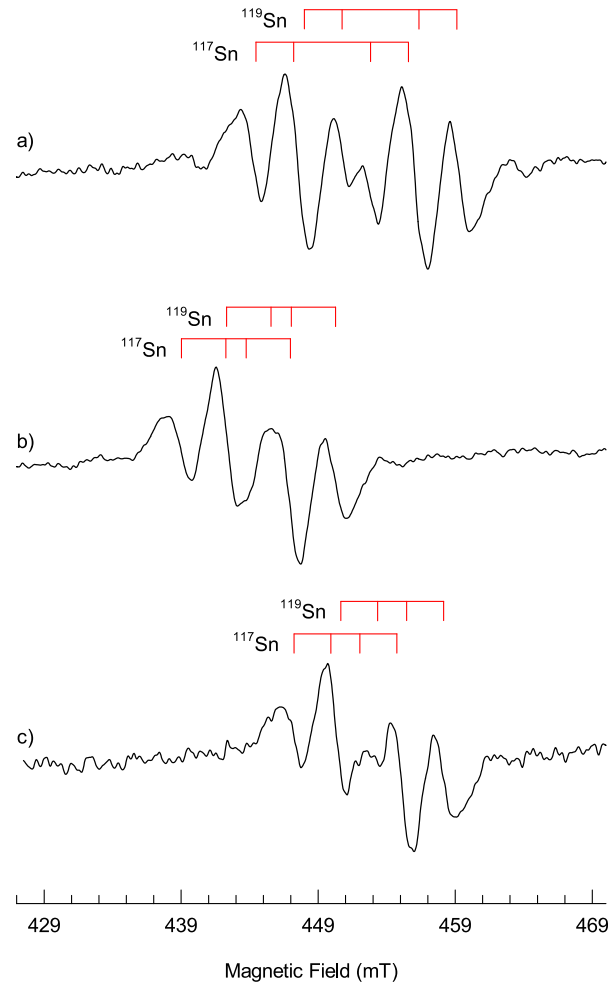

FIG. 2. High-field portions of the EPR spectra from the Sn vacancies in SPS. Stick diagrams show the [117]Sn and [119]Sn hyperfine lines from one Sn site. These data were taken at 90 K with a microwave frequency of 9.649 GHz. (a) The magnetic field is along the *a* direction in the crystal. (b) The magnetic field is along the *b* direction. (c) The magnetic field is along the *c* direction.

because the magnitudes of the Sn hyperfine interactions (between 8.2 and 8.8 GHz) never exceed our microwave fre-quency (9.39 GHz). The large Sn hyperfine interactions and their related large second-order effects in the spin Hamiltonian
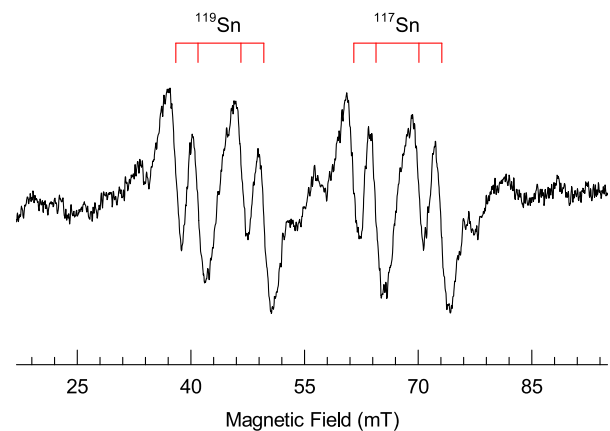

FIG. 3. Low-field portion of the Sn-vacancy EPR spectrum. Stick diagrams show the [117]Sn and [119]Sn hyperfine lines from one Sn site. These data were taken at 90 K with a microwave frequency of 9.392 GHz. The magnetic field is along the *a* direction in the crystal.

are responsible for the $I = 1/2$ high- and low-field [117,119]Sn lines being located asymmetrically about the $I = 0$ center lines in Fig. 1 (i.e., the Sn hyperfine lines do not form a symmetrical pattern about the more intense V_{Sn}^- lines at $g \approx 2.0$).

B. Spin-Hamiltonian parameters

The singly ionized charge state of the Sn vacancy (V_{Sn}^-) in $Sn_2P_2S_6$ crystals is described by the following $S = 1/2$ spin Hamiltonian:

$$H = \beta \mathbf{S} \cdot \mathbf{g} \cdot \mathbf{B} + \sum_i (\mathbf{I}_i \cdot \mathbf{A}_i \cdot \mathbf{S} - g_{n,i}\beta_n \mathbf{I}_i \cdot \mathbf{B}). \quad (1)$$

Electron Zeeman, hyperfine, and nuclear Zeeman terms are included with the summation being over all the ^{31}P, [117]Sn, and [119]Sn nuclei interacting with the unpaired electron. Relative abundances of the participating nuclei must be accounted for when predicting spectra using this Hamiltonian.

The g matrix and the hyperfine matrices for the two ^{31}P interactions were obtained by measuring the line positions within the central "$g \approx 2.0$" group of EPR lines (see Fig. 1) while rotating the magnetic field relative to the crystal axes. Data were taken every $15°$ in three planes (*a-b*, *b-c*, and *c-a*). These experimental results are plotted as discrete points in Fig. 4. In the monoclinic structure of the SPS crystal with its mirror plane perpendicular to the *b* axis, a paramagnetic point defect can have two crystallographically equivalent orientations, i.e., sites. These orientations are magnetically equivalent when the field is along the *a*, *b*, or *c* directions, and they are magnetically equivalent for all angles when the field is rotated in the *a-c* plane. As expected, Fig. 4 shows that there is a splitting into two branches in the *b-c* plane and no splitting into two branches in the *a-c* plane. The unexpected lack of a detectable splitting into two branches in the *a-b* plane in Fig. 4 implies that at least the *g* matrix and the larger ^{31}P hyperfine matrix in the spin-Hamiltonian have one of their principal-axis directions near the *a* direction.

The spin Hamiltonian from Eq. (1), with a *g* matrix and two ^{31}P hyperfine matrices, was rewritten in the form of an 8×8 matrix, and then was repeatedly diagonalized as the values of the 18 parameters were varied during a least-squares fitting. Six parameters define each matrix (i.e., three principal values and three Euler angles that specify the directions of the principal axes), thus giving the 18 parameters. Input data for the fitting process were 80 magnetic field values (the discrete data points in Fig. 4) and their corresponding microwave frequencies. Final sets of best-fit values for these parameters are listed in Table I. The solid lines in Fig. 4 were computer-generated using these principal values and principal-axis directions. In Table I, each set of three Euler angles describing the three principal-axis directions of a matrix has been converted to three (θ, ϕ) pairs. The polar angle θ is defined relative to the *c* axis of the crystal and the azimuthal angle ϕ is defined relative to the *a* axis with positive rotation from *a* toward *b* in the plane perpendicular to *c*. The signs of the ^{31}P principal values are not experimentally determined (we suggest in Table I that they are positive because the magnetic moment of the ^{31}P nucleus is positive).

A complete angular dependence of the [117]Sn and [119]Sn hyperfine lines associated with the Sn vacancy (V_{Sn}^-) was not acquired; instead, the values of these hyperfine parameters were only determined when the magnetic field was along the *a*, *b*, and *c* directions in the crystal. This is an appropriate and sufficient approach because the [117]Sn and [119]Sn matrices are nearly isotropic, thus making it difficult to extract meaningful information about the directions of the principal axes from an angular study. Specifically, midpoints of the low-field [117]Sn and [119]Sn groups of hyperfine lines were measured for the three "orthogonal" directions (these sets of lines are shown in Fig. 3 when the magnetic field is along the crystal's *a* direction). The experimental low-field positions were then used to determine values for the corresponding Sn hyperfine parameters. Because of significant second-order shifts, values for the Sn interactions were obtained by
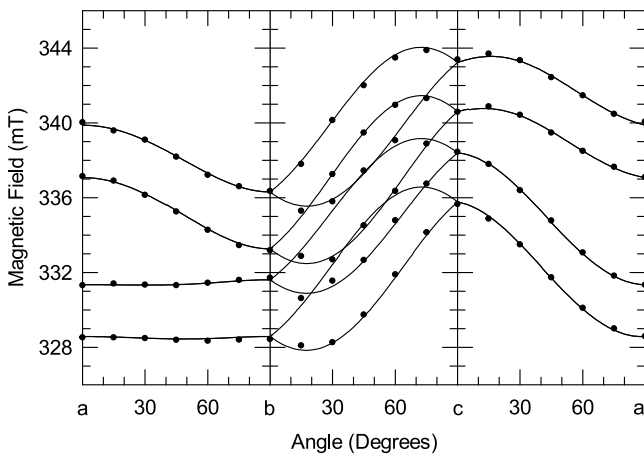

FIG. 4. EPR angular dependence of the singly ionized Sn vacancy in SPS. The *g* matrix and the ^{31}P matrices from two P sites are included. Positions of lines are plotted as a function of angle for rotations in the *a-b*, *b-c*, and *c-a* planes. Solid curves were calculated using the parameters in Table I and a microwave frequency of 9.393 GHz. Discrete points are experimental results.

TABLE I. Spin-Hamiltonian parameters for the ground state of the singly ionized Sn vacancy (V_{Sn}^-) in $Sn_2P_2S_6$ crystals. Units for the hyperfine parameters are in MHz. Uncertainties are estimated to be ± 0.0005 for the *g* values, ± 2.0 MHz for the A values, and $\pm 3°$ for the angles. Relative signs of the hyperfine parameters were not determined.

	Principal values	Principal-axis directions	
		θ (deg)	ϕ (deg)
g matrix			
g_1	2.0079	91.9	2.6
g_2	2.0231	72.4	92.0
g_3	1.9717	17.7	278.6
A hyperfine matrix (larger ^{31}P interaction)			
A_1	244.0	77.1	359.9
A_2	132.8	98.7	87.9
A_3	124.3	15.7	144.7
A hyperfine matrix (smaller ^{31}P interaction)			
A_1	87.5	69.3	74.2
A_2	82.5	116.0	153.6
A_3	67.7	34.2	197.8

matching observed line positions with solutions of a 4×4 spin Hamiltonian that included the *g* matrix (from Table I) and either a ^{117}Sn or ^{119}Sn isotropic hyperfine matrix. The resulting ^{117}Sn and ^{119}Sn values are listed in Table II. We used the low-field Sn hyperfine spectra to determine these Sn parameters because the positions of these lines are more sensitive to variations in the magnitudes of the ^{117}Sn and ^{119}Sn hyperfine values than the positions of lines in the high-field spectra (e.g., the significant overlap of these latter lines can be seen in Fig. 2). Negative signs are assigned to the hyperfine values in Table II because the magnetic moments of the ^{117}Sn and ^{119}Sn nuclei are negative and their hyperfine matrices are mostly isotropic.

C. Model of the Sn vacancy (V_{Sn}^-)

The spin-Hamiltonian parameters determined in Section III B provide the necessary information to establish a model for the ground state of the Sn vacancy (V_{Sn}^-) in SPS crystals. These EPR results clearly show that this $S = 1/2$ defect has principal *g* values very near 2.0 and primary hyperfine interactions with ^{31}P nuclei at two P sites and with ^{117}Sn and ^{119}Sn nuclei at one Sn site. At the beginning of our investigation, two possible models for the paramagnetic Sn vacancy (V_{Sn}^-) were thought to be viable. In one model, the unpaired spin (i.e., the hole) would be located on a Sn^{2+} ion adjacent to the Sn vacancy (this is analogous to the holelike small polaron[32] in SPS where the hole is stably trapped, at temperatures below ~65 K, on a Sn^{2+} ion and forms a Sn^{3+} ion). In the other model, the unpaired spin (i.e., the hole) would be located on the $(P_2S_6)^{4-}$ anionic unit adjacent to the Sn vacancy and form a $(P_2S_6)^{3-}$ unit. Our results show that the actual model is a combination of these two simpler models. The observation of significant hyperfine interactions with the ^{31}P nuclei at two P sites and the ^{117}Sn and ^{119}Sn nuclei at one Sn site provides experimental evidence that the unpaired spin is delocalized and overlaps both the Sn^{2+} ion and the $(P_2S_6)^{4-}$ unit that are next to the Sn vacancy. Hybridization of Sn valence electron orbitals with $(P_2S_6)^{4-}$ molecular orbitals[5,24] allows this sharing of the unpaired spin by the Sn^{2+} ion and $(P_2S_6)^{4-}$ unit.

A schematic model for the ground state of the Sn vacancy (V_{Sn}^-) is illustrated in Fig. 5. This model is meant to be descriptive, as we cannot experimentally distinguish whether the Sn vacancy is at a Sn1 or Sn2 crystallographic site.[33] For either position of the vacancy, the electronic structure of the V_{Sn}^- defect will be essentially the same because of the near-equivalence of these two Sn sites. In Fig. 5, the Sn
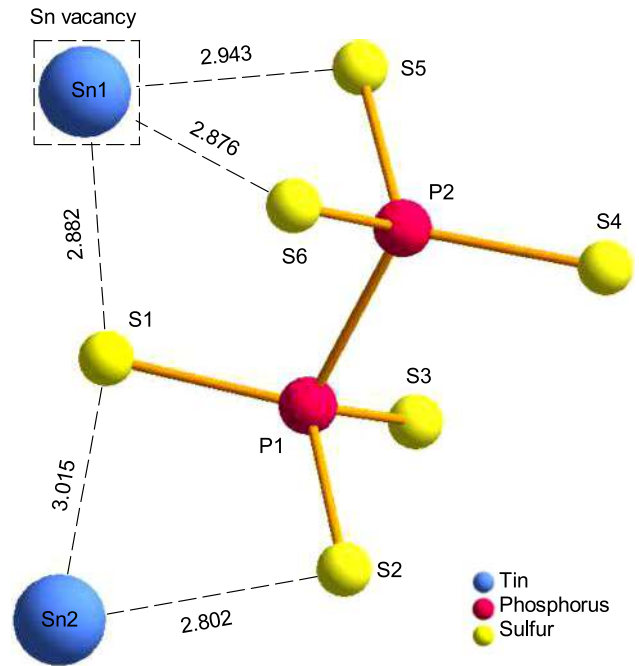

FIG. 5. The Sn vacancy and its neighboring ions in a $Sn_2P_2S_6$ crystal. A $(P_2S_6)^{4-}$ anionic unit and two nearby Sn^{2+} ions are shown in a projection along the "[111]" direction for this monoclinic lattice. If the vacancy is at the Sn1 site, then magnetic nuclei at the P1, P2, and Sn2 sites give rise to the observed hyperfine interactions. Relevant Sn-S distances (in Å units) are indicated by the dashed lines.

vacancy is located at the Sn1 position and the observed hyperfine interactions are with nuclei at the P1, P2, and Sn2 sites. The Sn1 site, as indicated in Fig. 5, is close to three sulfur ions (S1, S5, and S6), while the Sn2 site is close to only two sulfur ions (S1 and S2). These five separation distances range from 2.802 to 3.015 Å, and reflect the sum of the ionic radii of Sn^{2+} and S^{2-} ions for sixfold coordination (the Sn^{2+} radius is 1.18 Å and the S^{2-} radius is 1.84 Å). The electrostatic (Coulomb) energy of the defect is minimized when the trapped hole, which is, to a large extent, distributed over the sulfur ions within the (P_2S_6) unit, is as close as possible to the effective negative charge of the Sn vacancy. Having Sn1 close to three of the S ions, as opposed to only two of the S ions for Sn2, suggests that the vacancy may be at the Sn1 site since this will minimize the Coulomb energy. Unfortunately, we also cannot experimentally determine which of the two phosphorus nuclei (P1 or P2) has the larger ^{31}P hyperfine interaction. Because the two ^{31}P hyperfine interactions are not equivalent (see Table I), the wave function for the hole must be asymmetrically distributed over the (P_2S_6) unit. However, without knowing the detailed nature of the molecular orbitals and where the Sn vacancy is located, we cannot determine which P ion has the larger hyperfine interaction.

Making use of its more ionic nature, the percentage of unpaired 5*s* spin density on the adjacent Sn ion can be estimated from the isotropic Fermi contact portion of the ^{117}Sn and ^{119}Sn hyperfine parameters in Table II. Using $a = (A_1 + A_2 + A_3)/3$ and assuming that the A values all have the same sign, we find that $a = -8308$ MHz for the ^{117}Sn nuclei and $a = -8700$ MHz for the ^{119}Sn nuclei. Morton and Preston[36]

TABLE II. Observed Sn hyperfine interactions for the ground state of the singly ionized Sn vacancy (V_{Sn}^-) in $Sn_2P_2S_6$ crystals. These results were obtained from the low-field EPR spectra taken with the magnetic field along the *a*, *b*, and *c* directions (for example, see Fig. 3). They represent the interactions with ^{117}Sn and ^{119}Sn nuclei at one Sn site. Units are in MHz. Estimated uncertainty in each hyperfine value is ±5 MHz.

	a direction	*b* direction	*c* direction
A(^{117}Sn)	−8343	−8301	−8281
A(^{119}Sn)	−8733	−8694	−8674

predicted that a Sn 5s orbital (100% occupied) will have a value of $a = -43\,920$ MHz for the ^{119}Sn nuclei. Comparing our experimental result with this prediction for ^{119}Sn suggests that approximately 19.8% of the unpaired spin associated with the singly ionized Sn vacancy is located in a 5s orbital at the neighboring Sn site. Similarly, the hyperfine parameters in Table II can be used to make an estimate of the unpaired spin density in the 5p orbital on the Sn ion. The parameter b that describes the anisotropic part of the Sn hyperfine matrices is taken to be one-third of the difference between the largest and smallest hyperfine values for a given nucleus in Table II. This gives $b = -19.7$ MHz for the ^{119}Sn nuclei. Morton and Preston[36] predicted that a Sn 5p orbital (100% occupied) will have a value of $b = -732.4$ MHz for the ^{119}Sn nuclei (i.e., 2/5 of -1831 MHz). A comparison of these values for ^{119}Sn indicates that approximately 2.7% of the unpaired spin density is in a 5p orbital at the neighboring Sn site. Including both the s and p orbital contributions, our analysis suggests that 22.5% of the unpaired spin density is located on the neighboring Sn ion. This leaves most of the remaining 77.5% of the spin density on the primary P_2S_6 unit.

When coupled with our present experimental results, we anticipate that advanced density-functional-theory (DFT) calculations will provide a more detailed description of the ground state of the singly ionized Sn vacancy (V_{Sn}^-) in SPS crystals. A computational study will identify the primary molecular orbital(s) occupied by the unpaired spin. Also, these minimum-energy calculations may determine which Sn site is vacant, the location of the Sn ion responsible for the observed ^{117}Sn and ^{119}Sn hyperfine interactions, and which of the two phosphorus sites is responsible for the larger observed ^{31}P hyperfine interaction.

D. Activation energy

The singly ionized Sn vacancies in SPS become unstable (i.e., they thermally decay) if the laser light is removed when the temperature of the crystal is above approximately 105 K. Figure 6 shows the isothermal EPR decay curves taken at 107.5, 110, 112.5, and 115 K. These data were obtained with the magnetic field along the b direction and held constant at 331.0 mT. This value of magnetic field corresponds to the upper peak of the second EPR hyperfine line in Fig. 1(b). For each decay curve, the intensity of this specific EPR line was monitored as a function of time after turning off the 633 nm laser light. The temperature was kept constant (within ±0.05 K) while acquiring a set of decay data. The approximate initial concentrations of Sn vacancies were 7.58×10^{18}, 6.93×10^{18}, 5.71×10^{18}, and 5.24×10^{18} cm^{-3} at 107.5, 110, 112.5, and 115 K, respectively. These initial concentrations of V_{Sn}^- centers represent an equilibrium between their production rate (which depends on the intensity of the incident laser beam) and their decay rate (which depends on the temperature). The relative concentration values corresponding to the four temperatures are determined to within approximately 1% because we directly compare the defect's EPR spectrum taken with the same spectrometer settings and only slightly different temperatures. The absolute value of the spin concentration at 107.5 K was determined by comparing the spectrum from the
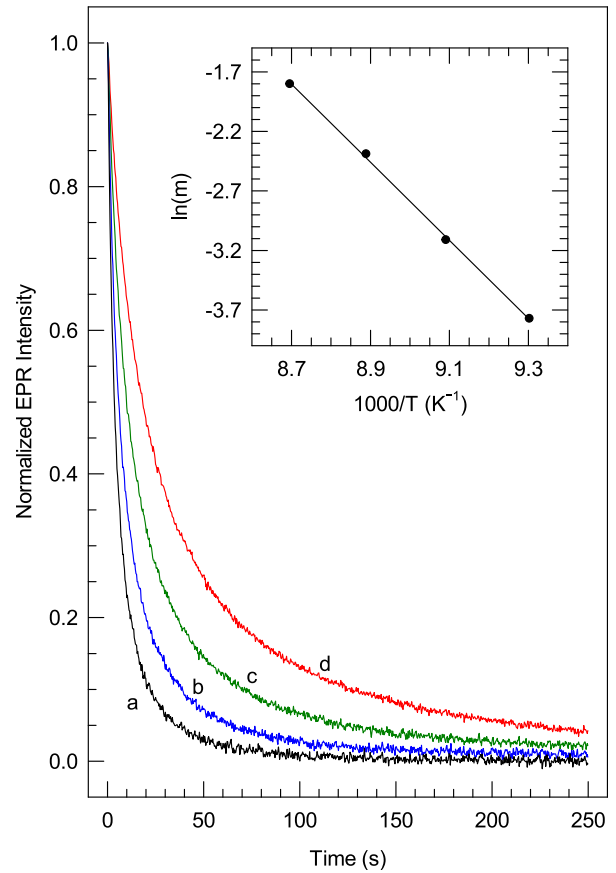

FIG. 6. Isothermal decay curves of the singly ionized Sn vacancy (V_{Sn}^-). Temperatures for the individual decay curves are (a) 115, (b) 112.5, (c) 110, and (d) 107.5 K. The inset shows the plot of ln(m) versus 1/T used to obtain the activation energy E.

defect with the spectrum of the standard pitch sample provided by Bruker (different linewidths, microwave powers, number of resolved lines, etc., were taken into account). This latter process is less precise and we estimate that the absolute value is only determined to within a factor of two.

First-order kinetics do not provide a good fit to the individual decay curves in Fig. 6 (i.e., these curves are not single exponentials). Thus, we use a general-order kinetics model[37] that takes into account the retrapping of thermally released charge to determine an activation energy for the thermal decay of these photoinduced singly ionized Sn vacancies. This analysis starts with the following differential equation:

$$\frac{dn}{dt} = -s'n^b \exp(-E/kT). \qquad (2)$$

Here, n is the concentration of defects, t is the time, b is the parameter which describes the order of the kinetics, E is the activation energy, and T is the temperature. In this general-order equation, the prefactor s' does not have units of inverse seconds. The solution to Eq. (2), for $b > 1$, is

$$n(t) = n_0 \left[1 + s'n_0^{b-1}(b-1)\exp(-E/kT)\,t \right]^{\frac{1}{1-b}}, \qquad (3)$$

where n_0 represents the initial concentration of singly ionized Sn vacancies (when the laser light is removed). Equation (3) is then rewritten in the following form:

$$\left(\frac{n}{n_0}\right)^{1-b} = \left[1 + s'n_0^{b-1}(b-1)\exp(-E/kT)t\right]. \quad (4)$$

Using the experimental data in Fig. 6, the quantity $(n/n_0)^{1-b}$ was plotted versus time for each decay curve. For each of these plots, the value of b was adjusted until a straight line emerged. The four values of b obtained from this procedure were very similar and their average was $b = 1.68$. This value of b indicates that the kinetics is between the first order and the second order. Each of the four straight lines has a different slope. From Eq. (4), these slopes are

$$m_i' = s'n_{0,i}^{b-1}(b-1)\exp(-E/kT_i), \quad (5)$$

where the index $i = 1$ to 4 corresponds to the four different temperatures where decay curves were obtained. As explained earlier, each decay curve has a different value of n_0 (for the same intensity of excitation light, the initial concentration of V_{Sn}^- centers is larger at the lower temperatures). Thus, we write $n_{0,i} = c_i N_0$ where the values of c_i are 1.00, 1.09, 1.32, and 1.45 for the 115, 112.5, 110, and 107.5 K decay curves, respectively (here, N_0 represents the initial concentration for the 115 K decay curve). Equation (5) then becomes

$$m_i = \frac{m_i'}{(c_i^{b-1})} = s'N_0^{b-1}(b-1)\exp(-E/kT_i). \quad (6)$$

Equation (6) can be rewritten in the following form by taking the natural logarithm of each side

$$\ln(m_i) = \ln\left[s'N_0^{b-1}(b-1)\right] - \frac{E}{kT_i}. \quad (7)$$

The final step is to construct a plot of $\ln(m_i)$ versus $1/T_i$ (this plot contains four points, one for each decay curve, and is shown in the inset of Fig. 6). The slope of the best-fit straight line in the inset is $-E/k$. Based on the thermal decay data in Fig. 6, our general-order kinetics analysis gives an activation energy of $E = 283$ meV. An estimate of the uncertainty in this value of E is ± 15 meV.

We now turn to the physical meaning of this activation energy. The effect of the 633 nm light is to produce acceptors (the Sn vacancy) with a trapped hole and donors (e.g., Sb impurities or sulfur vacancies) with a trapped electron. Upon removal of the light, these electrons and holes recombine and the original distribution of charge is restored, slowly or quickly depending on the temperature. The recombination process may be initiated by the thermal release of holes from the acceptor or the thermal release of electrons from a donor, and it is often difficult to determine whether the measured activation energy is associated with the hole release or the electron release. In the present case, we suggest that this activation energy of 283 meV describes the thermal release of a hole from the singly ionized Sn vacancy (V_{Sn}^-). These mobile holes quickly move to donors and recombine with trapped electrons. Experimentally, after removing the excitation light, we see that the singly ionized Sn vacancies (trapped holes) completely disappear within a few minutes in the 110–115 K region, whereas less than 25% of the singly ionized sulfur vacancies (trapped electrons) disappear as the Sn vacancies decay. These sulfur vacancies completely disappear after a few minutes at higher temperatures (in the 120–130 K range). The Sb^{2+} trapped electrons do not significantly decay (i.e., disappear) until near 200 K. These observations strongly suggest that hole release from the Sn vacancies is controlling the recombination process in the 110–115 K range. The opposite process, where the 283 meV activation energy is associated with the thermal release of an electron, would require the singly ionized sulfur vacancies to completely disappear in the 110–115 K range, in disagreement with the experiment.

IV. SUMMARY

Electron paramagnetic resonance (EPR) is used to identify and characterize the ground state of the singly ionized Sn vacancies in single crystals of $Sn_2P_2S_6$. The crystals in the present study are strongly compensated (with sulfur vacancies and inadvertently present Sb ions on Sn sites serving as the donors). In the as-grown crystals, the Sn vacancies are in their doubly ionized charge state (V_{Sn}^{2-}). Stable paramagnetic singly ionized Sn vacancies (V_{Sn}^-) are formed during an illumination below 100 K with 633 nm laser light, as the electrons are moved from the Sn-vacancy acceptors to the donors. Resolved hyperfine interactions with nuclei at two P sites and one Sn site indicate that the unpaired spin is delocalized over a Sn^{2+} ion and a $(P_2S_6)^{4-}$ anionic unit adjacent to the Sn vacancy (with approximately 22.5% of the unpaired spin density on the Sn^{2+} ion and 77.5% on the $(P_2S_6)^{4-}$ unit). After removing the laser light, these V_{Sn}^- trapped-hole defects become thermally unstable when the temperature is raised above 100 K. Using general-order kinetics, the thermal activation energy is estimated to be 283 meV.

[1]L. N. Dzhavadov and V. N. Ryzhov, Solid State Commun. **236**, 23 (2016).
[2]K. A. Brekhov, K. A. Grishunin, D. V. Afanas'ev, S. V. Semin, N. E. Sherstyuk, G. Kh. Kitaeva, E. D. Mishina, Th. Rasing, and A. V. Kimel, JETP Lett. **102**, 372 (2015).
[3]P. Ondrejkovic, M. Guennou, M. Kempa, Y. Vysochanskii, G. Garbarino, and J. Hlinka, J. Phys.: Condens. Matter **25**, 115901 (2013).
[4]P. Ondrejkovic, M. Kempa, Y. Vysochanskii, P. Saint-Grégoire, P. Bourges, K. Rushchanskii, and J. Hlinka, Phys. Rev. B **86**, 224106 (2012).
[5]K. Glukhov, K. Fedyo, J. Banys, and Y. Vysochanskii, Int. J. Mol. Sci. **13**, 14356 (2012).
[6]Y. Skrypka, A. Shumelyuk, S. Odoulov, S. Basun, and D. Evans, Opt. Commun. **356**, 208 (2015).
[7]A. Shumelyuk, A. Volkov, S. Odoulov, A. Grabar, I. Stoyka, and D. R. Evans, Opt. Express **22**, 24763 (2014).

[8]A. Grabar, P. Mathey, and G. Gadret, J. Opt. Soc. Am. B **31**, 980 (2014).

[9]P. Mathey, G. Gadret, A. Grabar, I. Stoika, and Y. Vysochanskii, Opt. Commun. **300**, 90 (2013).

[10]A. Volkov, A. Shumelyuk, S. Odoulov, and M. Imlau, J. Opt. Soc. Am. B **30**, 1102 (2013).

[11]A. Shumelyuk, M. Imlau, V. Dieckmann, H. Badorreck, A. Grabar, and S. Odoulov, Opt. Lett. **37**, 4065 (2012).

[12]A. Grabar, P. Mathey, and R. Iegorov, Appl. Phys. B **105**, 813 (2011).

[13]M. Imlau, V. Dieckmann, H. Badorreck, and A. Shumelyuk, Opt. Mater. Express **1**, 953 (2011).

[14]D. R. Evans, A. Shuymelyuk, G. Cook, and S. Odoulov, Opt. Lett. **36**, 454 (2011).

[15]A. Shumelyuk and S. Odoulov, J. Opt. **12**, 104015 (2010).

[16]A. Shumelyuk, A. Volkov, S. Odoulov, G. Cook, and D. R. Evans, Appl. Phys. B **100**, 101 (2010).

[17]A. Shumelyuk, S. Odoulov, G. Cook, and D. R. Evans, Opt. Lett. **34**, 2126 (2009).

[18]A. Shumelyuk, M. Wesner, M. Imlau, and S. Odoulov, Appl. Phys. B **95**, 497 (2009).

[19]I. V. Kedyk, P. Mathey, G. Gadret, A. A. Grabar, K. V. Fedyo, I. M. Stoika, I. P. Prits, and Y. M. Vysochanskii, Appl. Phys. B **92**, 549 (2008).

[20]T. Bach, M. Jazbinsek, G. Montemezzani, P. Gunter, A. A. Grabar, and Y. M. Vysochanskii, J. Opt. Soc. Am. B **24**, 1535 (2007).

[21]B. Sturman, P. Mathey, H. R. Jauslin, S. Odoulov, and A. Shumelyuk, J. Opt. Soc. Am. B **24**, 1303 (2007).

[22]M. Jazbinsek, D. Haertle, G. Montemezzani, P. Gunter, A. A. Grabar, I. M. Stoika, and Y. M. Vysochanskii, J. Opt. Soc. Am. B **22**, 2459 (2005).

[23]S. G. Odoulov, A. N. Shumelyuk, U. Hellwig, R. A. Rupp, A. A. Grabar, and I. M. Stoyka, J. Opt. Soc. Am. B **13**, 2352 (1996).

[24]Y. Vysochanskii, M. Medulych, A. Molnar, K. Glukhov, A. Dziaugys, J. Banys, R. Yevych, and M. Maior, Ferroelectrics **462**, 117 (2014).

[25]Y. Vysochanskii, A. Molnar, R. Yevych, K. Glukhov, and M. Medulych, Ferroelectrics **440**, 31 (2012).

[26]Y. Vysochanskii, K. Glukhov, M. Maior, K. Fedyo, A. Kohutych, V. Betsa, I. Prits, and M. Gurzan, Ferroelectrics **418**, 124 (2011).

[27]Y. Vysochanskii, K. Glukhov, K. Fedyo, and R. Yevych, Ferroelectrics **414**, 30 (2011).

[28]J. A. Weil and J. R. Bolton, *Electron Paramagnetic Resonance: Elementary Theory and Practical Applications*, 2nd ed. (John Wiley and Sons, New York, New York, 2007).

[29]J.-M. Spaeth and H. Overhof, *Point Defects in Semiconductors and Insulators: Determination of Atomic and Electronic Structure from Paramagnetic Hyperfine Interactions*, Springer Series of Materials Science Vol. 51 (Springer, Berlin, 2003).

[30]E. M. Golden, S. A. Basun, A. A. Grabar, I. M. Stoika, N. C. Giles, D. R. Evans, and L. E. Halliburton, J. Appl. Phys. **116**, 244107 (2014).

[31]A. T. Brant, L. E. Halliburton, S. A. Basun, A. A. Grabar, S. G. Odoulov, A. Shumelyuk, N. C. Giles, and D. R. Evans, Phys. Rev. B **86**, 134109 (2012).

[32]A. T. Brant, L. E. Halliburton, N. C. Giles, S. A. Basun, A. A. Grabar, and D. R. Evans, J. Phys.: Condens. Matter **25**, 205501 (2013).

[33]G. Dittmar and H. Schäfer, Z. Naturforsch. **29b**, 312 (1974).

[34]B. Scott, M. Pressprich, R. D. Willet, and D. A. Cleary, J. Solid State Chem. **96**, 294 (1992).

[35]K. Kuepper, B. Schneider, V. Caciuc, M. Neumann, A. V. Postnikov, A. Ruediger, A. A. Grabar, and Yu. M. Vysochanskii, Phys. Rev. B **67**, 115101 (2003).

[36]J. R. Morton and K. F. Preston, J. Magn. Reson. **30**, 577 (1978).

[37]S. Yang, A. T. Brant, N. C. Giles, and L. E. Halliburton, Phys. Rev. B **87**, 125201 (2013).